EUROPHYSICS LETTERS

OFFPRINT

Vol. 69 • Number 4 • pp. 538–543

Optical near-field of multipolar plasmons of rod-shaped gold nanoparticles

* * *

A. Hohenau, J. R. Krenn, G. Schider, H. Ditlbacher, A. Leitner, F. R. Aussenegg and W. L. Schaich

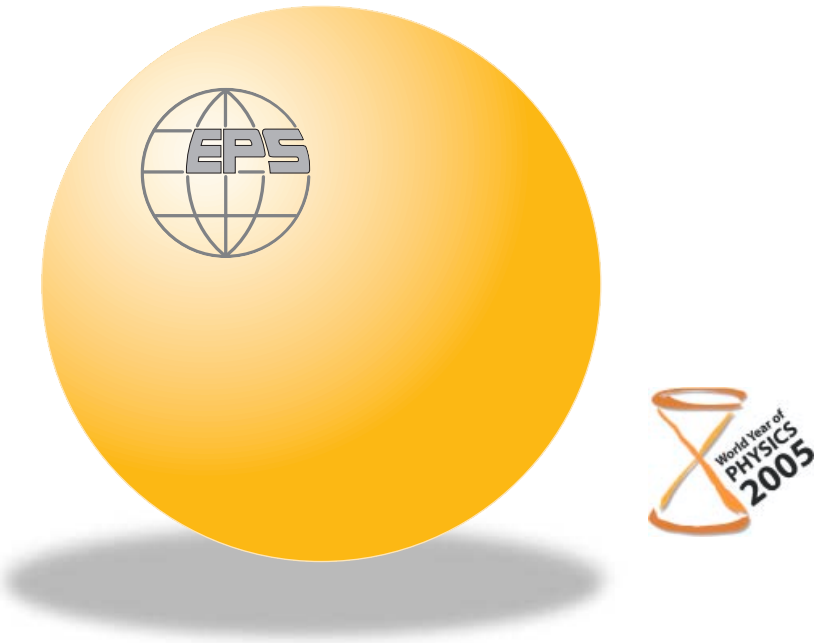

Published under the scientific responsability of the
EUROPEAN PHYSICAL SOCIETY
Incorporating
JOURNAL DE PHYSIQUE LETTRES • LETTERE AL NUOVO CIMENTO

EDP SCIENCES

EUROPHYSICS LETTERS

Europhysics Letter was launched more than fifteen years ago by the European Physical Society, the Société Française de Physique, the Società Italiana di Fisica and the Institute of Physics (UK) and owned now by 17 National Physical Societies/Institutes.

Europhysics Letters aims to publish short papers containing non-trivial new results, ideas, concepts, experimental methods, theoretical treatments, etc. which are of broad interest and importance to one or several sections of the physics community.

Europhysics letters provides a platform for scientists from all over the world to offer their results to an international readership.

Subscription 2005

24 issues - Vol. 69-72 (6 issues per vol.)

ISSN: 0295-5075 - ISSN electronic: 1286-4854

- France & EU (VAT included) ☐ 1 795 €
- Rest of the World (without VAT) ☐ 1 795 €

Payment:

❒ Check enclosed payable to EDP Sciences

❒ Please send me a pro forma invoice

❒ Credit card:

❒ Visa ❒ Mastercard ❒ American Express

Valid until: |_|_|_|_|

Card No: |_|_|_|_|_|_|_|_|_|_|_|_|_|_|_|_|

Signature:

❒ Please send me a **free** sample copy

Institution/Library: . . . . . .
. . . . . .
Name: . . . . . .
Position: . . . . . .
Address: . . . . . .
. . . . . .
. . . . . .
ZIP-Code: . . . . . .
City: . . . . . .
Country: . . . . . .
E-mail: . . . . . .

Order through your subscription agency or directly from EDP Sciences:
17 av. du Hoggar • B.P. 112 • 91944 Les Ulis Cedex A • France
Tel. 33 (0)1 69 18 75 75 • Fax 33 (0)1 69 86 06 78 • subscribers@edpsciences.org

Europhys. Lett., **69** (4), pp. 538–543 (2005)
DOI: 10.1209/epl/i2004-10388-9

Optical near-field of multipolar plasmons of rod-shaped gold nanoparticles

A. Hohenau[1], J. R. Krenn[1], G. Schider[1], H. Ditlbacher[1], A. Leitner[1], F. R. Aussenegg[1] and W. L. Schaich[2]

[1] *Institute for Experimental Physics and Erwin Schrödinger Institute for Nanoscale Research, Karl-Franzens-University Graz - A-8010 Graz, Austria*
[2] *Department of Physics, Indiana University - Bloomington, IN 47405, USA*

received 30 August 2004; accepted in final form 10 December 2004
published online 19 January 2005

PACS. 42.25.Hz – Wave optics: Interference.
PACS. 73.20.Mf – Collective excitations (including excitons, polarons, plasmons and other charge-density excitations).
PACS. 78.67.Bf – Optical properties of bulk materials and thin films: Nanocrystals and nanoparticles.

Abstract. – We report on near-field measurements and calculations of the optical intensity close to rod-shaped gold nanoparticles excited at a multipolar plasmon resonance. Our results reveal a distinct optical near-field pattern and show that multipolar plasmon excitation of single nanoparticles can be imaged in the near-field. The observed optical near-field patterns can be understood in a model of standing plasmon waves.

Nanoparticles composed of the noble metals gold or silver can sustain resonant, coherent electron plasma oscillations. These excitations are commonly termed "particle plasmons" and can be excited by light in the visible and near-infrared spectral regions [1]. For a given metal and surrounding medium the spectral resonance position is determined by the nanoparticle size and shape. Particle plasmon excitation gives rise to absorption and scattering cross-sections exceeding the geometric particle dimensions and an electromagnetic near-field enhancement up to 400 times the incident-field amplitude [2].

These properties make the study of noble-metal nanoparticles an attractive field for fundamental and applied research. Their absorption and scattering properties enable optical filter, colour pigment and security feature applications [3]; while their strong near-fields may be exploited to enhance surface Raman scattering [4], fluorescence for, *e.g.*, ultra-sensitive detection of biomolecules [3] and the efficiency of optical nonlinear effects [5]. Moreover, particle plasmons are promising candidates for the realization of nano-optical devices [6].

Up to now, research has mainly concentrated on the lowest (dipolar) particle plasmon mode. However, for a complete understanding of particle plasmon properties the higher-order (multipolar) modes must also be taken into account [1]. These multipolar modes can differ strongly from the dipolar mode in terms of spectral and near-field properties. Besides the fundamental research aspect, the analysis of multipolar particle plasmons might therefore contribute significantly to expanding the application range of metal nanoparticles.

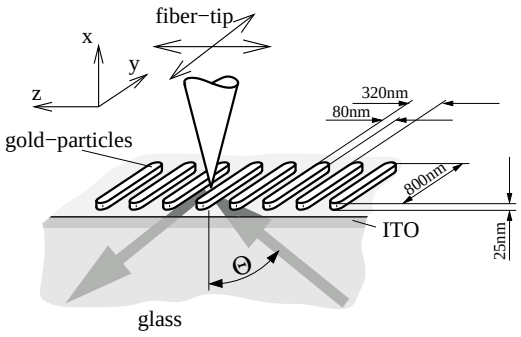

Fig. 1 – Sketch of the sample and the excitation and detection scheme. The gold nanoparticles are excited from the glass-side under total internal reflection ($\Theta = 48°$) with TE-polarized ($\boldsymbol{E}$ parallel to y) light. The optical near-field is probed by an uncoated dielectric fiber tip which is scanned over the sample.

While a few reports on optical spectroscopy of multipolar particle plasmon modes have been published recently [7, 8], little is known about the optical near-field pattern corresponding to these modes. In this letter, we report on the direct imaging by optical near-field microscopy of multipolar particle plasmon modes in elongated gold nanoparticles. Our experimental results agree well with calculations based on an analytical model that also provides insight into the physical nature of these modes.

We investigate elongated (rod-shaped) gold nanoparticles arranged in ordered planar arrays (fig. 1). The samples are fabricated by electron-beam writing of a computer designed pattern into a poly-methyl-methacrylate resist layer spin-coated onto indium-tin-oxide (ITO) doped glass substrates. Chemical development of the resist, vacuum deposition of gold and, finally, removal of gold at the unexposed areas by a liftoff process follow sequentially [9]. The resulting gold nanoparticles lie on top of the ITO-doped glass substrates, surrounded by air. For a given particle width and height, the design length is chosen so that a particle plasmon resonance is energetically located within the spectral tuning range of the cw titanium:sapphire laser we use as the excitation source for the optical near-field measurements.

Far-field extinction spectra of the samples are measured with a Zeiss *MMS1* micro-spectrometer, integrated into a Zeiss *Axioscope* optical microscope. The spectra are acquired at normal incidence with a 2.5×, 0.075 numerical aperture objective. Optical near-field intensity images are recorded by a custom-built photon scanning tunnelling microscope [10]. The sample is fixed with index matching fluid on a BK7 glass prism and optical excitation is accomplished by weakly focusing the laser beam into the prism (angle of incidence $\Theta = 48°$). The focal full width at half-maximum is approximately 300 μm, and the polarization of the beam is chosen so that the electric field vector is perpendicular to the plane of incidence. For the near-field probe we use an uncoated chemically etched tip of a 820 nm mono-mode optical fiber (3M) glued to a 32 kHz quartz tuning fork [11]. The fiber tip is scanned over the sample and held at constant distance from the surface by shear force feedback [11]. The light intensity output of the fiber is detected by a photomultiplier, amplified and recorded as a function of the lateral coordinates of the fiber tip. The detected signal is proportional to the optical near-field intensity to good approximation [12]. However, uncoated dielectric tips are capable of coupling propagating light modes outside the fiber via their cone to a guided mode within the fiber. Therefore special care has to be taken to suppress propagating light modes in the region of the fiber tip.

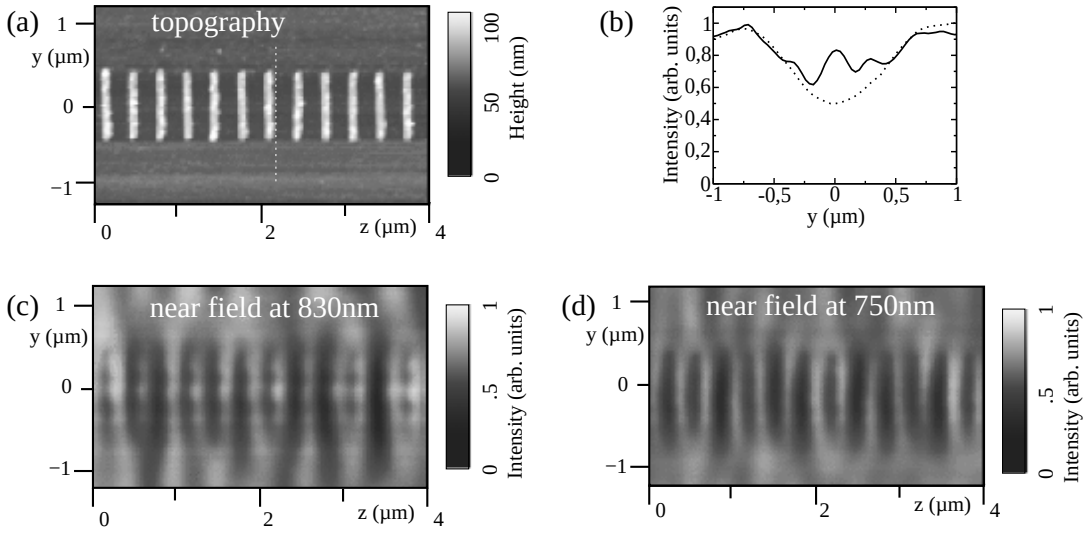

Fig. 2 – Topography (a) and near-field optical intensity maps of an array of nanoparticles excited at $\lambda_0 = 830$ (c) and 750 nm (d); part (b) shows the near-field intensity of (c) and (d) above the dashed line indicated in (a). The polarization of the excitation is parallel to the long particle axis (y-direction).

We accomplish this by 1) using optical excitation at an angle larger than the critical angle of total internal reflection (fig. 1) and 2) arranging the particles in an array with a small grating constant ($d_z = 320$ nm) such that no grating orders can be diffracted into the half-space above the sample surface. In the orthogonal direction we choose a grating constant $d_y = 2\,\mu$m.

Figure 2 shows the topographical image of the sample (a), consisting of an array of nanoparticles with approximate dimensions of $25 \times 800 \times 80$ nm. Near-field optical images (acquired simultaneously with the topographical data) are displayed for excitation wavelengths of $\lambda_0 = 830$ nm (c) and 750 nm (d). Two patterns dominate the near-field images: First, pronounced fringes parallel to the long particle axis (this fringe pattern has less intensity over the particles than in between them, *i.e.*, it shows negative contrast) and second, in the case of fig. 2(c) ($\lambda_0 = 830$ nm), a three-maxima pattern along the long particle axis (fig. 2(b)). Comparig fig. 2(a) and (c) reveals that there are virtually no topographically induced artifacts in the near-field images [13].

To identify the optical excitation conditions we present in fig. 3 the far-field extinction spectrum (dashed line) of the sample at normal incidence. For the chosen polarization parallel to the long particle axis two distinct extinction maxima are present in the covered spectral range. This data (acquired for perpendicular incidence) can be directly correlated with the near-field data (angle of incidence $\Theta = 48°$) since particles orientated perpendicular to the plane of incidence are subject to only slight variations in the exciting light field for particle cross-section dimensions small compared to the light wavelength. The dependence of the particle plasmon resonance location on the angle of incidence should hence be negligible.

We now calculate the extinction spectrum with a method of moments that assumes the induced current in the particles may be treated as two-dimensional (in the plane of the interface). For the calculation the particle grating is considered to be infinite and the particles are treated as negligibly thin with a sheet resistance derived from the dielectric function of gold and the particle height. This approach was recently applied successfully to similar problems [14,15]. It

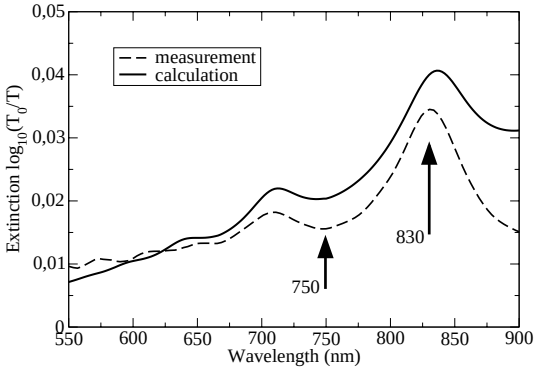

Fig. 3 – Experimental (dashed line) and calculated (solid line) extinction spectra of the investigated array of nanoparticles at normal incidence for a polarization parallel to the long particle axis. The arrows indicate the excitation wavelengths used to acquire and calculate the on- ($\lambda_0 = 830\,\mathrm{nm}$) and off-resonance ($\lambda_0 = 750\,\mathrm{nm}$) optical near-field images.

leads to the physical picture that optical resonances in our samples are due to standing waves of current along the long particle axis. Following this interpretation, we can assign standing plasmon waves of order 5 and 7 as the primary cause of the two extinction peaks observed in the calculated spectrum (solid line in fig. 3) at $\lambda_0 = 830\,\mathrm{nm}$ and $\lambda_0 = 710\,\mathrm{nm}$, respectively. In the calculations we account for the optical response of the ITO-doped glass substrate [16] and make modest changes in the nanoparticle geometric parameters, which are set to $24 \times 830 \times 70\,\mathrm{nm}$. The correspondence of measured and calculated extinction spectra is good.

Next consider the optical near-field patterns. In fig. 4 the optical near-field intensity for an array of gold nanoparticles as calculated from our model is depicted. The calculations take no direct account of the presence of the near-field probe. The intensity is computed at a fixed height $x_0 = 140\,\mathrm{nm}$ above the surface, which was shown in earlier work to correspond to an effective detection height for the fiber tips we use [17, 18]. This scheme leads to calculated intensity profiles that compare well with the measured data of fig. 2. This agreement encourages us to examine further the physical content of our model and to develop a physical interpretation of the observed intensity pattern.

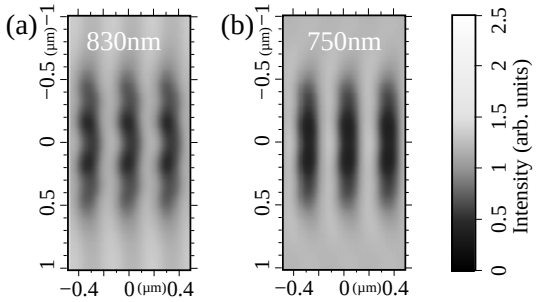

Fig. 4 – Calculated near-field maps for a grating of rod-like gold nanoparticles. The excitation wavelengths are chosen identical to the experimental cases, while the geometry is that used in fig. 1. The plotted quantity is $|\boldsymbol{E}|^2$ at a height 140 nm above the surface. The middle particle is centered on $y = z = 0$.

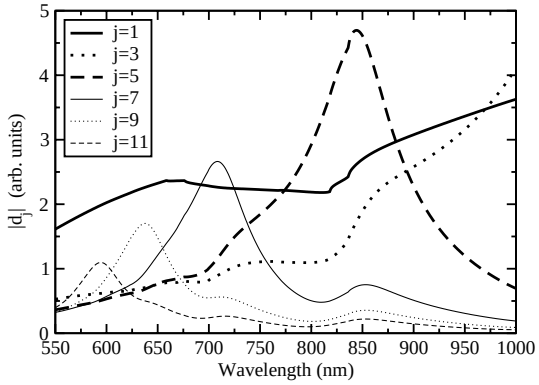

Fig. 5 – Calculated strength of the different excited current amplitudes $|d_j|$ in a particle. The case $j = 5$ has its resonance near $\lambda_0 = 830\,\mathrm{nm}$, where however also other odd-j amplitudes of comparable strength are present. The even-j amplitudes are zero for our excitation geometry [15].

As discussed above, we chose the periods of our grating array to be small enough to prevent propagating diffraction orders from emerging into the air space above the nanoparticles. However, the grating structure does generate structured evanescent fields whose decay with vertical distance from the particles is faster the more rapid their lateral variations are. As a consequence, at the effective detection height, x_0, the optical field corresponding to the resonantly excited fifth-order standing plasmon wave has already decayed more than contributions due to non-resonant diffraction from the nanoparticle array and the evanescent field of the totally reflected excitation beam. An estimate of the magnitude of the non-resonant, grating-induced fields is possible from fig. 5, which shows the calculated spectral dependence of the standing current wave amplitudes d_j [14]. Each d_j multiplies $\cos(j\frac{\pi y}{w_y})\theta(\frac{w_y}{2} - |y|)\theta(\frac{w_z}{2} - |z|)$ in an expansion of the current along y, for a nanoparticle centred on the origin. Here w_y (w_z) is the particle length (width) and the θ-functions restrict the current to within the particle boundaries. The index j sets the standing-wave order.

Even at the $j = 5$ resonance ($\lambda_0 \approx 830\,\mathrm{nm}$) the non-resonant $|d_j|$'s are of comparable magnitude. As a consequence, the fluctuating field at x_0 associated with, say, d_5 is, although resonant, always small compared to the smoother, non-resonant fields. The net effect is that the fine structure of $|\boldsymbol{E}|^2$ at x_0 is determined by an interference between (small) resonant and (large) non-resonant field contributions:

$$I = |\boldsymbol{E}|^2 \approx |E_y|^2 + 2\,\mathrm{Re}\left(E_y\ \delta E_y^\star\right), \tag{1}$$

where Re(...) denotes "real part of" (...) and E_y (δE_y) is the non-resonant (resonant) contribution. The intensity profile due to E_y alone is structured in both the z and y directions and is basically the structure appearing off-resonance in fig. 4. The modulations that appear on resonance in fig. 4 come from the interference term, linear in δE_y which in turn is roughly proportional over each particle to $\cos(j\frac{\pi y}{w_y})$ with $j = 5$. The net effect is that near resonance one observes additional peaks only where δE_y is maximum (assuming $E_y > 0$), instead of all the places where $|\delta E_y|^2$ is maximum. This explains why a $j = 5$ resonance can lead to only 3 peaks in the near-field intensity profile and clarifies that the obtained images are due to an interference of the evanescent exciting field and the fields of resonantly and non-resonantly excited plasmon modes. The images can therefore not be directly interpreted in terms of the optical near-field intensity of the particle eigenmodes [19].

In conclusion, we have shown that it is possible to image the optical near-field of gold nanoparticles excited at a multipolar plasmon resonance. By interpreting these modes in terms of standing current waves, we found good quantitative agreement with the experimental observations and gained qualitative insight into the observed physical processes. On the one hand, these results significantly broaden the spectrum of potential plasmonic applications with a wider range of near-field patterns and resonance frequencies compared to the well-known dipolar plasmon resonance. On the other hand, we have also identified experimental restrictions due to the important role of non-resonant plasmon excitations.

REFERENCES

[1] Kreibig U. and Vollmer M., *Optical Properties of Metal Clusters*, Vol. **25** (Springer) 1995.
[2] Kottmann J. P., Martin J. F., Smith D. R. and Schitz S., *Opt. Express*, **6** (2000) 213.
[3] Bauer G., Hassmann J. W., Haglmüller J., Mayer C. and Schalkhammer T., *Nanotechnology*, **14** (2003) 1289.
[4] Chang R. K. and Furtak T. E. (Editors), *Surface Enhanced Raman Scattering* (Plenum Press, New York) 1982.
[5] Aussenegg F. R., Leitner A. and Gold H., *Appl. Phys. A*, **60** (1995) 97.
[6] Quinten M., Leitner A., Krenn J. R. and Aussenegg F. R., *Opt. Lett.*, **23** (1998) 1331.
[7] Krenn J. R., Schider B., Rechberger W., Lamprecht B., Leitner A., Aussengg F. R. and Weeber J. C., *Appl. Phys. Lett.*, **77** (2000) 3379.
[8] Oldenburg S. J., Hale G. D., Jackson J. B. and Halas N. J., *Appl. Phys. Lett.*, **8** (1999) 1063.
[9] McCord M. A. and Rooks M. J., *Handbook of Microlithography, Micromachining and Microfabrication*, Vol. **1** (SPIE and The Institution of Electrical Engineers, Bellingham, Washington) 1997, Sect. 2, pp. 139-249.
[10] Krenn J. R., Lamprecht B., Ditlbacher H., Schider G., Salerno M., Leitner A. and Aussenegg F. R., *Europhys. Lett.*, **60** (2003) 663.
[11] Karrai K. and Grober R. D., *Appl. Phys. Lett.*, **66** (1995) 1842.
[12] Dereux A., Girard C. and Weeber J. C., *J. Chem. Phys.*, **112** (2000) 7775.
[13] Hecht B., Bielefeldt H., Inouye Y., Pohl D. W. and Novotny L., *J. Appl. Phys.*, **81** (1997) 2492.
[14] Schaich W. L., Schider G., Krenn J., Leitner A., Aussenegg F. R., Puscasu I., Monacelli B. and Boreman G., *Appl. Opt.*, **42** (2003) 5714.
[15] Schider G., Krenn J. R., Hohenau A., Ditlbacher H., Leitner A., Aussenegg F. R., Schaich W. L., Puscasu I., Monacelli B. and Boreman G., *Phys. Rev. B*, **68** (2003) 155427.
[16] Synowicki R. A., *Thin Solid Films*, **313-314** (1998) 349.
[17] Krenn J. R., Weeber J. C., Dereux A., Bourillot E., Goudonnet J. P., Schider B., Leitner A., Aussenegg F. R. and Girard C., *Phys. Rev. B*, **60** (1999) 5029.
[18] Krenn J. R., Dereux A., Weeber J. C., Bourillot E., Lacroute Y., Goudonnet J. P., Schider G., Gotschy W., Leitner A. and Aussenegg F. R., *Phys. Rev. Lett.*, **82** (1999) 2590.
[19] Weeber J. C., Dereux A., Girard C. G., Krenn J. R. and Goudonnet J. P., *Phys. Rev. B*, **60** (1999) 9061.